Available online at www.sciencedirect.com
SCIENCE DIRECT
ELSEVIER
Solid State Communications 136 (2005) 108–113
solid state communications
www.elsevier.com/locate/ssc

The correlation between structure and magnetic properties in the manganites $La_{0.7}Ca_{0.3-x}Te_xMnO_3$ ($0 \leq x \leq 0.15$)

J. Yang[a], Y.Q. Ma[a], W.H. Song[a], R.L. Zhang[a], B.C. Zhao[a], Y.P. Sun[a,b,*]

[a]*Key Laboratory of Materials Physics, Institute of Solid State Physics, Chinese Academy of Sciences, Hefei 230031, People's Republic of China*
[b]*National Laboratory of Solid State Microstructures, Nanjing University, Nanjing 210008, People's Republic of China*

Received 7 February 2005; received in revised form 9 May 2005; accepted 6 June 2005 by A.K. Sood
Available online 16 June 2005

Abstract

The effect of Te-doping at La-site on structural, magnetic and transport properties in the manganites $La_{0.7}Ca_{0.3-x}Te_xMnO_3$ ($0 \leq x \leq 0.15$) has been investigated. All samples show an orthorhombic structure (O'-*Pbnm*) at room temperature. It shows that the Mn–O–Mn bond angle decreases and the Mn–O bond length increases with the increase in the Te content. All samples exhibit an insulator–metal (I–M) transition and the resistivity increases with the increase in the Te-doping level. Additionally, the Curie temperature T_c decreases and the transition becomes broader with increasing Te-doping level, in contrast, the magnetization of Te-doping samples at low temperatures decrease with increasing x as $x \leq 0.10$ and then increase with further increasing x to 0.15. The results are discussed in terms of Jahn–Teller (JT) vibrational anisotropy Q_3/Q_2 and the opening of the new DE channel between Mn^{2+}–O–Mn^{3+} due to the introduction of Mn^{2+} ions because of the substitution of Te^{4+} ions for Ca^{2+} ions.

PACS: 75.30.Kz; 75.47.Lx; 71.30+h

Keywords: A. Colossal magnetoresistance; D. Magnetic properties; D. Electrical transport

1. Introduction

The hole-doped magnanites $Ln_{1-x}A_xMnO_3$ (Ln=La–Tb, and A=Ca, Sr, Ba, Pb, etc.) have attracted much renewed attention because of their peculiar electrical transport and magnetic properties, especially the property of colossal magnetoresistance (CMR), which is promising for their potential applications such as magnetic reading heads, field sensors and memories [1–3]. Extensive research has been done on metallic, ferromagnetic (FM) manganites of the type $La_{0.7}Ca_{0.3}MnO_3$, through the doping at La^{3+} sites with trivalent rare earths (Y [4–7], Pr [5], Ho [6], Dy [8–10], Tb [11,12], etc.) or divalent elements (Sr [13], etc.) with different sizes keeping the fixed Ca concentration (at 0.3) close to an optimum value in relation to the FM interaction. These substitutions bring about strong lattice and disorder effects, and ultimately influence the magnetic and transport properties of these materials. The lattice distortion introduced by La-site disorder influences the FM double exchange (DE) couplings by changing the Mn–O–Mn bond angle and Mn–O bond length. Phenomenologically, the changes in the magnetic and transport behaviors can be understood in terms of the tolerance factor t for the perovskite structure, i.e. the average ionic size of the La-site, and the La-site size disorder, i.e. the width σ of the distribution of the ions on the La site [14–16]. Apart from the above factors, some researches [17–19] suggest that the Jahn–Teller (JT) distortion strongly affects the magnetic structure. Rivadulla et al. [20] point out that the cooperative

* Corresponding author. Address: Key Laboratory of Materials Physics, Institute of Solid State Physics, Chinese Academy of Sciences, P.O. Box 1129, Hefei 230031, People's Republic of China. Tel.: +86 5515592757; fax: +86 5515591434.
E-mail address: ypsun@issp.ac.cn (Y.P. Sun).

0038-1098/$ - see front matter © 2005 Elsevier Ltd. All rights reserved.
doi:10.1016/j.ssc.2005.06.009

rotation of the MnO_6 octahedra determines the vibrational anisotropy between JT modes (Q_3/Q_2), and subsequently affects the magnetic structure in orthomanganites (O'-*Pbnm*). Recently, some researches place emphasis on the tetravalent ion doping at La-site and find some interesting phenomena, depending on the nature of the substitution cation. Strong frustrated magnetism was observed in $La_{0.47}Ce_{0.20}Ca_{0.33}MnO_3$ [21]. Mn ordering and induced Ce ordering was reported in $La_{0.7}$ $(Ce_{0.5}Ca_{0.5})_{0.3}MnO_3$ [22]. Kondo-like effect was found in the DE ferromagnet $La_{0.5-x}Ce_xSr_{0.5}MnO_3$ [23]. Ce is a rare-earth element and the compound $La_{0.7}Ce_{0.3}MnO_3$ also shows CMR effect [24]. Therefore, it is of great interest to investigate the structural, transport and magnetic properties in the compound $La_{0.7}Ca_{0.3}MnO_3$ in which a tetravalent element in chalcogen rather than rare-earth element is partially substituted at La-sites. In the previous studies, the electron-doped manganites $La_{1-x}Te_xMnO_3$ [25], $La_{0.9-x}Pr_xTe_{0.1}MnO_3$ [26] and $La_{0.85}Te_{0.15}Mn_{1-x}Cu_xO_3$ [27] show some interesting phenomena. These investigations also suggest that the CMR behavior probably occurs in the mixed-valent state of Mn^{2+}/Mn^{3+}. The basic physics in terms of Hund's rule coupling between e_g electrons and t_{2g} core electrons and JT effect due to Mn^{3+} JT ions can operate in the electron-doped manganites as well. In this paper, we investigate the structural, magnetic and transport properties in the Te-doped manganites $La_{0.7}Ca_{0.3-x}Te_xMnO_3$ ($0 \le x \le 0.15$) and find that the magnetic properties is closely related to the structural properties and the results are interpreted in terms of the JT vibrational anisotropy.

2. Experiment

$La_{0.7}Ca_{0.3-x}Te_xMnO_3$ samples with nano-scale grains were prepared by a citrate gel technique [28], since this procedure can enhance the density and phase homogeneity of the samples at lower temperatures. Stoichiometric amounts of high-purity La_2O_3, $CaCO_3$, and TeO_2 powders were dissolved in diluted nitric acid in which an excess of citric acid was added, followed by the addition of stoichiometric amounts of $Mn(NO_3)_2$ dissolved in deionized water with continuous stirring, and then ethylene glycol was added to make a solution complex. After all the reactants had been completely dissolved, the solution was heated on a hot plate resulting in the formation of a gel. The gel was dried at 250 °C, and then preheated to 600 °C to remove the remaining organic matter and decompose the nitrates of the gel. The obtained powders were ground, pelletized, and sintered at 1100 °C for 24 h, and finally, the furnace was slowly cooled down to the room temperature.

The crystal structures were examined by X-ray diffractometer using Cu K_α radiation at room temperature. The magnetic measurements were carried out with a quantum design superconducting quantum interference device (SQUID) MPMS system ($2 \le T \le 400$ K, $0 \le H \le 5$ T). Zero-field-cooled (ZFC) data was recorded. The resistance was measured by the standard four-probe method from 25 to 300 K.

3. Results and discussion

The powder X-ray diffraction at room temperature shows that all samples are single phase with no detectable secondary phases and the samples have an orthorhombic structure with the space group *Pbnm*. The structural parameters of the samples are refined by the standard Rietveld technique [29]. In the process of refinement, the substitution of Te ions at La sites was considered. As an example, one of the fitted pattern ($x=0.15$) is shown in Fig. 1 and no structure transition has been found, meaning that the substitution takes place in a disordered way. Detailed results of the structural refinements are listed in Table 1. As we can see, the lattice parameters of $La_{0.7}Ca_{0.3-x}Te_xMnO_3$ samples vary monotonously with increasing the Te-doping level. The Mn–O–Mn bond angle ($\theta_{Mn-O-Mn}$) decreases with the increase in the Te, whereas, the Mn–O bond length (d_{Mn-O}) displays the inverse correlation to the variation in the Mn–O–Mn bond angle.

Fig. 2 shows the temperature dependence of resistivity $\rho(T)$ for the samples with $x=0$, 0.05, 0.10, and 0.15 at zero field in the temperature range of 30–300 K. For the sample with $x=0$, it shows that there exists an I–M transition at T_p(=260 K) and the transition near T_p is very sharp, which is the same as the result reported elsewhere [30]. For the samples with $x=0.05$, 0.10, and 0.15, the $\rho(T)$ curve exhibits single I–M transition at the temperature of 259, 255, and 224 K, respectively. Fig. 2 also shows that ρ increases with the increase in the Te-doping level and the resistivity of the sample with $x=0.15$ increases two orders of magnitude compared with that of the sample with $x=0$. We suggest that the remarkable increase in ρ for the Te-doping samples mainly originates from the introduction of random Coulomb

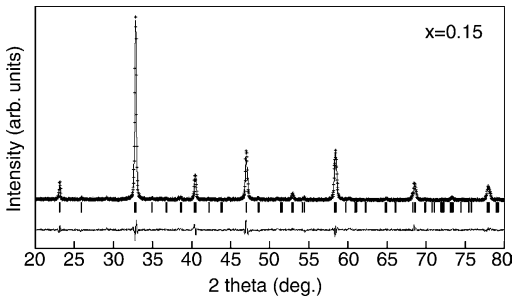

Fig. 1. The experimental and calculated XRD patterns of $La_{0.7}Ca_{0.3-x}Te_xMnO_3$ with $x=0.15$. Crosses indicate the experimental data and the calculated data is the continuous line overlapping them. The lowest curve shows the difference between experimental and calculated patterns. The vertical bars indicate the expected reflection positions.

Table 1
Refined structural parameters of $La_{0.7}Ca_{0.3-x}Te_xMnO_3$ ($0 \le x \le 0.15$) at room temperature

Parameter	$x=0$	$x=0.05$	$x=0.10$	$x=0.15$
a (Å)	5.4689(7)	5.4790(13)	5.4868(8)	5.5043(9)
b (Å)	5.4520(9)	5.4631(7)	5.4761(6)	5.4803(3)
c (Å)	7.7189(6)	7.7356(15)	7.7471(7)	7.7566(6)
v (Å^3)	230. 1492(7)	231. 4674(12)	232. 7974(5)	233. 9803(4)
Mn–O(1) (Å)	1.9560(2)	1.9644(2)	1.9791(1)	1.9702(1)
Mn–O(2) (Å)	1.9308(1)	1.9479(1)	1.9815(1)	2.0149(1)
Mn–O(2) (Å)	1.9755(2)	1.9691(1)	1.9402(1)	1.9353(2)
(Mn–O) (Å)	1.9541(2)	1.9605(1)	1.9669(1)	1.9735(1)
Mn–O(1)–Mn (°)	161.19(2)	159.78(1)	158.87(3)	159.64(2)
Mn–O(2)–Mn (°)	162.56(1)	161.85(1)	160.78(1)	158.94(1)
⟨Mn–O–Mn⟩ (°)	162.10(1)	161.16(1)	160.14(2)	159.17(1)
R_p (%)	9.81	8.39	7.60	7.90

O(1), apical oxygen; O(2), basal plane oxygen.

potential caused by the Te-doping at La-site. The experimental data measured at a magnetic field of 0.5 T for the samples with $x=0$, 0.05, 0.10 and 0.15 are also plotted in Fig. 2 denoted in dashed lines. It shows that the applied field suppressed the resistivity peak at T_p significantly and the resistivity peak shifts towards higher temperatures. The magnetoresistance (MR) as a function of temperature based on the data shown in Fig. 2 is plotted in Fig. 3. Here the MR is defined as $\Delta\rho/\rho_0=(\rho_0-\rho_H)/\rho_0$, where ρ_0 is the resistivity at zero fields and ρ_H is the resistivity at an applied magnetic field of 0.5 T. For all the samples, there are corresponding peaks in the vicinity of T_p on the MR curves, and then the MR values increase with

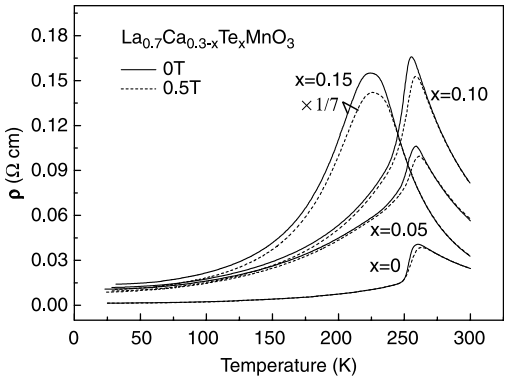

Fig. 2. The temperature dependence of the resistivity $\rho(T)$ for the samples with $x=0$, 0.05, 0.10, and 0.15 at zero (solid lines) and 0.5 T fields (dashed lines).

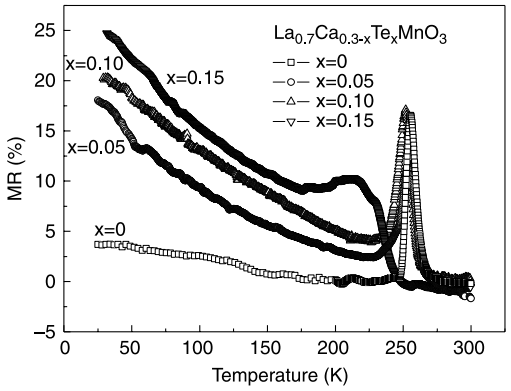

Fig. 3. The temperature dependence of magnetoresistance (MR) ratio for the samples with $x=0$, 0.05, 0.10, and 0.15 at $H=0.5$ T.

decreasing temperatures, which is similar to MR behavior observed usually in polycrystalline samples of electron-doped manganites which is considered to be related to grain boundaries [27].

The temperature dependence of magnetization M of $La_{0.7}Ca_{0.3-x}Te_xMnO_3$ ($0 \le x \le 0.15$) under ZFC mode at $H=0.1$ T are measured. Our measured samples may be considered as ellipsoid in which the demagnetized factor $N=0.05$ (SI units), and the applied field is parallel to the longest semi-axis of samples. So a uniform field can exist throughout the samples and the shape demagnetizing fields can be reduced as much as possible. The results are shown in the main panel of Fig. 4 for the samples with $x<0.15$. The Curie temperature T_c (defined as the one corresponding to the peak of dM/dT in the M vs. T curve) are 261, 258, 250, and 200 K for the samples with $x=0$, 0.05, 0.10, and 0.15, respectively, which are listed in Table 2. Obviously, the Curie temperature T_c decreases monotonously with increasing Te-doping level. We suggest that the T_c reduction should be attributed to the reduction of Mn–O–Mn bond angle, and thereby reducing the matrix element b that describes

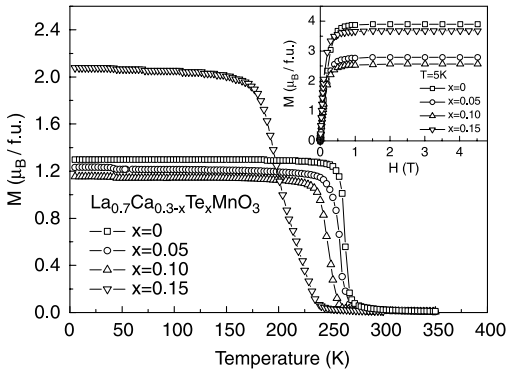

Fig. 4. Magnetization as a function of temperature $M(T)$ for the samples with $x=0$, 0.05, 0.10, and 0.15 under zero-field-cooled (ZFC) modes. The inset shows field dependence of the magnetization $M(H)$ for the samples with $x=0$, 0.05, 0.10, and 0.15 at 5 K.

Table 2
T_c, T_p and the fitting parameter of $La_{0.7}Ca_{0.3-x}Te_xMnO_3$ ($0 \le x \le 0.15$) samples

Parameter	$x=0$	$x=0.05$	$x=0.1$	$x=0.15$
T_c (K)	261	258	250	200
T_p (K)	260	259	255	224

electron hopping between Mn sites. Thus the DE interaction becomes weakening because of the narrowing of the bandwidth and the decrease in the mobility of e_g electrons due to the increase in Mn–O bond length and the decrease in Mn–O–Mn bond angle caused by the substitution of smaller Te^{4+} ions for larger Ca^{2+} ions. Then a salient question to ask is: what is the variation for the valence-state of Mn ions after substituting Ca^{2+} by Te^{4+}? We consider that the Te^{4+}-doping would introduce the Mn^{2+} ions on the basis of the following factors. On the one hand, the oxygen content of the samples was determined by a redox (oxidation reduction) titration. The detailed method to determine the oxygen content of samples is reported in elsewhere [32]. The oxygen content of all samples almost stabilizes around 3.01. On the other hand, if we suppose the Mn^{2+} ions would not be introduced, the composition of $La_{0.7}Ca_{0.3-x}Te_xMnO_3$ ($0 \le x \le 0.15$) can be written as $La_{0.7}Ca_{0.3-x}Te_xMn^{3+}_{0.7+2x}Mn^{4+}_{0.3-2x}O_3$. We can see that with the increase in x, the ratio of Mn^{4+}/Mn^{3+} would decrease. As a result, the Curie temperature T_c of the samples would decrease and accordingly the resistivity would increase, which seems to be consistent with the obtained results. As the Te-doping level reaches 0.15, the Mn^{4+} ion should disappear, how can the FM ordering accompanied by I–M transition occur in the compound $La_{0.7}Ca_{0.3-x}Te_xMn^{3+}O_3$? The FM Mn^{3+}–O–Mn^{3+} interactions can occur in the perovskites with O-orthorhombic or rhombohedral symmetry by the vibronic-induced Jahn–Teller (JT) effect proposed by Goodenough et al. [33]. Nevertheless the studied samples have the structure with O'-orthorhombic symmetry. Moreover, the 90° superexchange ferromagnetism (SFM) [34] that occurs in some compounds with no Mn mixed valence, i.e. $Tl_2Mn_2O_7$ [35] and $CaCu_3Mn_4O_{12}$ [36] compounds, cannot be used to account for the present sample because the Mn–O–Mn bond angle for the sample with $x=0.15$ is about 159°, which deviates obviously from 90°. Based on the above consideration, we suggest that the mixed-valence state of Mn^{2+}, Mn^{3+}, and Mn^{4+} would concur in the studied samples. Thus, the composition of $La_{0.7}Ca_{0.3-x}Te_xMnO_3$ can be written as $La_{0.7}Ca_{0.3-x}Te_xMn^{2+}_xMn^{3+}_{0.7}Mn^{4+}_{0.3-x}O_3$, which is satisfactory for explaining the structural, magnetic and transport properties. As we know, the radius of the Mn^{2+}, Mn^{3+}, and Mn^{4+} is 0.83, 0.645, and 0.53 Å in nine coordination conditions [37], respectively, that is to say, $R_{Mn^{4+}} < R_{Mn^{3+}} < R_{Mn^{2+}}$. As a result, when the amount of the Te^{4+} increases, the amount of the Mn^{4+} will decrease. At the same time the amount of the Mn^{2+} will increase giving rise to the increase in the Mn–O bond length and the decrease in the Mn–O–Mn bond angle. Thus the DE interaction weakens because of the narrowing of the bandwidth and T_c would decrease with the increase in the Te-doping level. Additionally, because the $La_{0.7}Ca_{0.3-x}Te_xMnO_3$ is a system with severe disorder due to the concurrence of different valence state and distinct ions (La^{3+}, Ca^{2+}, Te^{4+}, Mn^{2+}, Mn^{3+}, and Mn^{4+}) in the lattice and the disorder may lead to the carrier localization leading to the increase in the resistivity when the Te^{4+} ions are doped at La-site. In addition, from Fig. 4, a sharp FM to paramagnetic (PM) transition is observed in the samples with $x<0.1$. However, as $x=0.15$, the temperature range of FM–PM phase transition become broader implying a wider distribution of the magnetic exchange interactions in the Mn–O–Mn network, i.e. the increase in magnetic inhomogeneity. Although the decrease in T_c and broadening of PM–FM transition with increasing Te-doping level, the magnetization of the samples with $x=0.15$ increases at low temperatures compared with that of the samples with $x<0.1$. The magnetization as a function of the applied magnetic field at 5 K is shown in the inset of Fig. 4. The magnetization reaches saturation at about 1 T and keeps constant up to 4.5 T for all the samples, which is considered as a result of the rotation of the magnetic domain under external magnetic field. Additionally, similar to the results shown in the main panel of Fig. 4, the magnetization of Te-doping samples

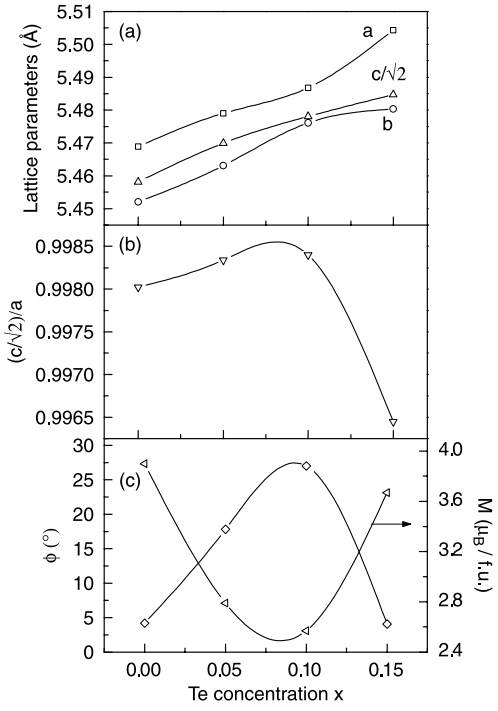

Fig. 5. (a) the lattice parameters, (b) the ration of $c/\sqrt{2})/a$, and (c) the JT vibrational anisotropy Φ and the magnetic moment at 5 K as a function of x for $La_{0.7}Ca_{0.3-x}Te_xMnO_3$ ($0 \le x \le 0.15$) samples.

decreases at low temperatures as $H>1$ T for $x<0.1$ compared with that of no Te-doped sample. It is noteworthy that the magnetization of the sample with $x=0.15$ increases at low temperatures compared with that of the samples with $0.05\leq x\leq 0.1$. It may be related to Jahn–Teller vibrational anisotropy. The opening of the new DE channel between Mn^{2+}–O–Mn^{3+} is also possible because the substitution of Te^{4+} for Ca^{2+} introduces Mn^{2+} ion.

The lattice parameters of the samples $La_{0.7}Ca_{0.3-x}Te_xMnO_3$ ($0\leq x\leq 0.15$) obtained from the fitted XRD data is shown in Fig. 5(a). We can see that the structure is O'-orthorhombic symmetry ($c/a<\sqrt{2}$). Additionally, the variation of the lattice parameters a, b and c is abnormal as $x=0.1$. To further characterize the variation of the lattice parameters, we show, in Fig. 5(b), the ratio of $(c/\sqrt{2})/a$ (or almost equivalently the ratio of the apical to equatorial Mn–O bond length) [38] as a function of doping level x for $La_{0.7}Ca_{0.3-x}Te_xMnO_3$. As seen in Fig. 5(b), the $(c/\sqrt{2})/a$ ratios increase smoothly with increasing x from 0 to 0.1, and then decrease abruptly with further increasing x to 0.15. It is well known that the degeneracy of the doublet e_g levels is lifted by tetragonal distortions of the MnO_6 octahedra with either Q_2 or Q_3 mode JT distortion. Q_2 is an orthorhombic distortion with the in-plane bonds differentiating in a long and a short one. Q_3 is the tetragonal distortion with the in-plane bond lengths shortening and the out-of-plane bonds extending. This c axis compressed or elongated lattices are obviously a manifestation of different types of JT distortions. In order to confirm this point, we show the JT vibration anisotropy Φ as a function of doping level x. Kanamori [39] shows that the ratio Q_3/Q_2 present in a given static distortion is $\tan\Phi=(2/\sqrt{6})(2m-l-s)/\pm(2/\sqrt{2})(l-s)$, where s and l are the short and long Mn–O bond lengths that alternate along [100] and [010] axes, m is the bond length along [001], $s\leq m\leq l$, and Φ is the angle between the state vectors and the Q_2 axis. In the high-anisotropy limit, $m=s$, only the Q_3 mode is present ($\Phi=30°$), whereas for the low-anisotropy case there is only Q_2. In fact, in real JT distorted materials, both the Q_2 and Q_3 modes contribute to the lattice distortion. Nevertheless, the ratio Q_3/Q_2 depends on the value of l, m and s. Using the Mn–O bond length at 300 K obtained from Rietveld analysis of our XRD data, we calculated the value of Φ. The x-dependence of the Φ is plotted in Fig. 5(c). It can be seen that, for $x=0$, $\Phi=4.27°$, indicating a modest anisotropy, which is similar to the results reported elsewhere [20]. Interestingly, when x increases from 0 to 0.1, the Φ increases almost linearly and evolves toward the high anisotropy ($\Phi=27.03°$ for $x=0.1$). The increase in Φ suggests a growth of Q_3 mode and a decrease in Q_2 mode. With further increasing x from 0.1, the Φ decreases abruptly ($\Phi=4.07°$ for $x=0.15$), indicating a modest anisotropy and the Q_2 being predominant mode for $x=0.15$. The interplay between JT distortion and magnetic structures has been studied by many groups [17–19], and their investigations suggest that JT vibrational anisotropy determines the magnetic structure in orthorhombic manganites. Rivadulla et al. [20] indeed found that the larger the Φ was, the lower the FM saturation moment was at 5 K. In order to show the interplay between the magnetic properties and JT vibrational anisotropy clearly, we also plotted the FM saturation moment at 5 K for the samples $La_{0.7}Ca_{0.3-x}Te_xMnO_3$ ($0\leq x\leq 0.15$) in the Fig. 5(c). We can see that the FM saturation moment displays the inverse correlation to the variation in the Φ. That is to say, for the samples $La_{0.7}Ca_{0.3-x}Te_xMnO_3$ ($0\leq x\leq 0.15$), the JT vibrational anisotropy determines the variation of FM saturation moment. For the sample with $x=0$, the JT distortion is modest corresponding to the large FM saturation moment. When x increase from 0 to 0.1, the anisotropy of JT distortion increases leading to the decrease in the FM saturation moment. With further increasing x to 0.15, the JT distortion is renewedly modest resulting in the increase in FM saturation moment.

Fig. 6 shows the temperature dependence of the inverse magnetic susceptibility χ_m for all samples. For ferromagnet, it is well known that in the PM region, the relation between χ_m and the temperature T should follow the Curie–Weiss law, i.e. $\chi_m=C/(T-\Theta)$, where C is the Curie constant, and Θ is the Weiss temperature. The lines in Fig. 6 are the calculated curves deduced from the Curie−Weiss equation. The Weiss temperature Θ is obtained to be 261, 253, 241, and 220 K for the samples with $x=0$, 0.05, 0.10, and 0.15, respectively. For the sample with $x=0$, Θ values is the same as its corresponding T_c value. For the samples with $x=0.05$ and 0.10, Θ values are lower than their corresponding T_c values, whereas for the sample with $x=0.15$, Θ value is higher than its T_c value, which may be related to the magnetic inhomgeneity. The Curie constant C deduced from the fitting data is 5.38, 4.46, 4.44 and 5.77 K cm^3/mol for the samples with $x=0$, 0.05, 0.10 and 0.15, respectively. And thus the effective magnetic moment μ_{eff} can be obtained as 3.28, 2.98, 2.97, and 3.39 μ_B for the samples with $x=0$,

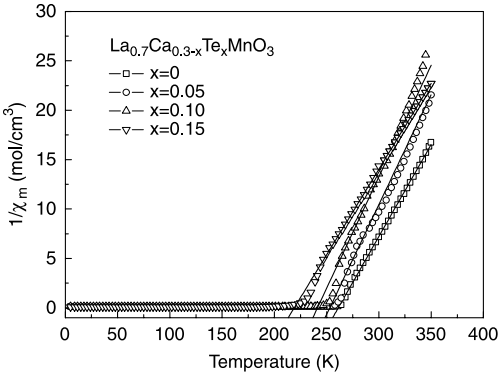

Fig. 6. The temperature dependence of the inverse of the magnetic susceptibility χ_m for the samples with $x=0$, 0.05, 0.10, and 0.15. The lines are the calculated curves according to the Curie-Weiss law (see text).

0.05, 0.10, and 0.15, respectively. As can be seen that, the effective magnetic moment μ_{eff} decreases with increasing x from $x=0$ to 0.1, then increasing with further increase in x. This variation is similar to the case of the saturated magnetic moment at 5 K, indicating in both cases, JT vibrational anisotropy both play an important role in determining the magnetic properties for the samples $La_{0.7}Ca_{0.3-x}Te_xMnO_3$. According to a mean field approximation [40], the expected effective magnetic moment μ_{eff} can also be calculated as 4.59, 4.69, 4.79, and 4.89 μ_B for the sample with $x=0$, 0.05, 0.10, and 0.15, respectively. These values are obviously larger than the fitted values from $1/\chi_m$–T curves. It implies that there may exist a strong spin-orbit coupling in $La_{0.7}Ca_{0.3-x}Te_xMnO_3$ ($0\leq x\leq 0.15$) leading to the gyromagnetic factor less than 2.

4. Conclusion

We have studied the structural, magnetic and transport properties for $La_{0.7}Ca_{0.3-x}Te_xMnO_3$ ($0\leq x\leq 0.15$). All samples exhibit an orthorhombic O' phase at room temperature. All samples show I–M transition at T_p and the resistivity increases with the increase in the Te-doping level, which is mainly related to the introduction of random Coulomb potential caused by the Te doping at La-site. Moreover, the Curie temperature T_c decreases with increasing the Te-doping level. Whereas, the magnetization of Te-doping samples at low temperatures decrease with increasing the Te-doping level as $x\leq 0.10$ and then increase with further increasing x to 0.15, which is presumably related to the variation of vibrational anisotropy Q_3/Q_2. The opening of the new DE channel between Mn^{2+}–O–Mn^{3+} is also possible because the substitution of Te^{4+} ions for Ca^{2+} ions introduces Mn^{2+} ions.

Acknowledgements

This work is supported by the National Key Basic Research under contract No. 001CB610604, and the National Nature Science Foundation of China under contract No.10174085, 10474100 and Anhui Province NSF Grant No. 03046201 and the Fundamental Bureau Chinese Academy of Sciences.

References

[1] (a) R. von Helmolt, et al., Phys. Rev. Lett. 71 (1993) 2331;
(b) A.P. Ramirez, J. Phys.: Condens. Matter 9 (1997) 8171;
(c) J.M.D. Coey, et al., Adv. Phys. 48 (1999) 167;
(d) M.B. Salamon, et al., Rev. Mod. Phys. 73 (2001) 583.
[2] K. Chahara, et al., Appl. Phys. Lett. 63 (1993) 1990.
[3] S. Jin, et al., Science 264 (1994) 413.
[4] R.S. Freitas, et al., Phys. Rev. B 64 (2001) 144404.
[5] H.Y. Hwang, et al., Phys. Rev. Lett. 75 (1995) 914.
[6] V. Ravindranath, et al., Phys. Rev. B 63 (2001) 184434.
[7] G. Alejandro, et al., J. Appl. Phys. 87 (2000) 5603.
[8] T. Terai, et al., Phys. Rev. B 58 (2001) 14908.
[9] S.M. Yusuf, et al., J. Alloys Compd. 326 (2001) 89.
[10] S.M. Yusuf, et al., Phys. Rev. B 68 (2003) 104421.
[11] J. Blasco, et al., J. Phys.: Condens. Matter 8 (1996) 7427.
[12] J.M. De Teresa, et al., Phys. Rev. B 56 (1997) 3317.
[13] J. Mira, et al., Phys. Rev. B 60 (1999) 2998.
[14] L.M. Rodriguez-Martinez, et al., Phys. Rev. B 54 (1996) R15622.
[15] L. Sheng, et al., Phys. Rev. B 59 (1999) 13550.
[16] L.M. Rodriguez-Martinez, et al., Phys. Rev. B 58 (1998) 2426.
[17] H. Sawada, et al., Phys. Rev. B 56 (1997) 12154.
[18] R.Y. Gu, et al., Phys. Rev. B 65 (2002) 214426.
[19] R.K. Zheng, et al., Appl. Phys. Lett. 83 (2003) 5250.
[20] F. Rivadulla, et al., Phys. Rev. B 64 (2001) 052403.
[21] G. Alejandro, et al., Phys. Rev. B 67 (2003) 064424.
[22] S.Y. Wu, et al., J. Magn. Magn. Mater. 239 (2002) 14.
[23] T. Eto, et al., J. Magn. Magn. Mater. 226–230 (2001) 879.
[24] J.R. Gebhardt, et al., J. Appl. Phys. 85 (1999) 5390.
[25] G.T. Tan, et al., Phys. Rev. B 68 (2003) 014426.
[26] J. Yang, et al., Phys. Rev. B 70 (2004) 144421.
[27] J. Yang, et al., Phys. Rev. B 70 (2004) 092504.
[28] (a) M. Verelst, et al., J. Solid State Chem. 104 (1993) 74;
(b) I.G. Deac, et al., Phys. Rev. B 65 (2002) 174426.
[29] D.B. Wiles, et al., J. Appl. Crystallogr. 14 (1981) 149.
[30] Y.Q. Ma, et al., Phys. Rev. B 69 (2004) 134404.
[32] J. Yang, et al., J. Magn. Magn. Mater. 285 (2005) 417.
[33] J.B. Goodenough, et al., Phys. Rev. 124 (1961) 373.
[34] J.B. Goodenough, Magnetism and the Chemical Bond, Interscience, New York, 1963.
[35] M.A. Subaramanian, et al., Science 273 (1996) 81.
[36] Z. Zeng, et al., Phys. Rev. B 58 (1998) R595.
[37] R.D. Shannon, Acta Crystallogr. Sect. A 32 (1976) 751.
[38] Y. Tokura, et al., Science 288 (2000) 462.
[39] J. Kanamori, Suppl. J. Appl. Phys. 31 (1960) 14S.
[40] S. de Brion, et al., Phys. Rev. B 59 (1999) 1304.